Cellular/Molecular

Distribution of K^+-Dependent Na^+/Ca^{2+} Exchangers in the Rat Supraoptic Magnocellular Neuron Is Polarized to Axon Terminals

Myoung-Hwan Kim,[1] Sang-hyuk Lee,[2] Kyeong Han Park,[2] Won-Kyung Ho,[1] and Suk-Ho Lee[1]
Departments of [1]Physiology and [2]Anatomy, Seoul National University College of Medicine, Chongno-Ku, Seoul, 110-799, Korea

Neurons are polarized into compartments such as the soma, dendrites, and axon terminals, each of which has highly specialized functions. To test whether Ca^{2+} is differently handled in different compartments of a neuron, we investigated Ca^{2+} clearance mechanisms in somata of supraoptic magnocellular neurosecretory cells (MNCs) and in their axon terminals located in neurohypophyses. Using patch-clamp and microfluorometry techniques, Ca^{2+} transients were evoked by depolarizing pulses. Endogenous Ca^{2+} binding ratios (κ_S) and Ca^{2+} clearance rates were calculated from the decay phases of Ca^{2+} transients according to the single compartment model. Mean values of κ_S were 79 ± 2.6 in somata of MNCs and 187 ± 19 in axon terminals. Ca^{2+} clearance rate in axon terminals, which were calculated from time derivative of Ca^{2+} decay and the κ_S values, were approximately threefold higher than in somata. In response to external Na^+ reduction, Ca^{2+} clearance rates were reduced by 65% in axon terminals, but did not change in somata. Immunohistochemical assays confirmed that K^+-dependent Na^+/Ca^{2+} exchanger (NCKX2) was specifically localized to neurohypophysial axon terminals and was not found in somata. In somata, inhibition of sarcoendoplasmic reticulum Ca^{2+}-ATPase (SERCA) pumps, mitochondrial Ca^{2+}-uniporter, and plasma membrane Ca^{2+}-ATPase (PMCA) pumps decreased Ca^{2+} clearance rate by 48, 27, and 21%, respectively. These results suggest that neurohypophysial axon terminals have greater Ca^{2+} clearance power than somata because of the specific localization of NCKX2, and that Ca^{2+} clearance in somata of MNCs is mediated by SERCA pumps, mitochondrial uniporter, and PMCA pumps.

Key words: **calcium clearance; supraoptic nucleus; neurohypophysis; NCKX; SERCA; mitochondria**

Introduction

Neurons are polarized into compartments such as the soma, dendrites and axon terminals, each of which has highly specialized functions. Calcium, the most universal intracellular messenger, may be differently handled in different compartments of a neuron. Various Ca^{2+} clearance mechanisms, such as plasma membrane Ca^{2+}-ATPase (PMCA), sarcoendoplasmic reticulum Ca^{2+}-ATPase (SERCA), Na^+/Ca^{2+} exchanger, and mitochondrial Ca^{2+} uniporter, have been described in neurons (for review, see Thayer et al., 2002), but most information stems from somata or axon terminals independently.

SERCA is thought to be the major mechanism of Ca^{2+} clearance in somata of cerebellar Purkinje neurons (Fierro et al., 1998) and the dendrites of cortical pyramidal neurons (Markram et al., 1995). Mitochondria have been reported to shape Ca^{2+} transients by buffering Ca^{2+} upstroke in dorsal root ganglion cells (Werth and Thayer, 1994). In axon terminals, contribution of Na^+/Ca^{2+} exchange (Reuter and Porzig, 1995), mitochondria (Billups and Forsythe, 2002), and PMCA (Zenisek and Matthews, 2000; Usachev et al., 2002) have been described in various neuronal cells. Taken together, these studies suggest that the relative contribution of each of these mechanisms to Ca^{2+} clearance varies widely among different mammalian neurons. It has, however, not yet been studied whether any of these mechanisms is preferentially localized to a specific region of a neuron, probably because the opportunities for direct comparison of Ca^{2+} clearance between the axon terminals and somata of the same cell are limited. In this respect, magnocellular neurosecretory cells (MNCs) in the supraoptic nucleus and axon terminals in the neurohypophyses (NHP) allow a unique opportunity to investigate the subcellular localization of Ca^{2+} clearance mechanisms.

We previously reported that the K^+-dependent Na^+/Ca^{2+} exchanger NCKX plays a dominant role (~60%) in Ca^{2+} clearance in the axon terminals of rat neurohypophyses (Lee et al., 2002). NCKX is thought to be an efficient Ca^{2+} clearance mechanism in photoreceptor, in which constant Na^+ influx threatens the transmembrane $[Na^+]$ gradient that is necessary for driving Ca^{2+} extrusion (Cervetto et al., 1989). Accordingly, we hypothesized that NCKX would be a suitable mechanism of Ca^{2+} clearance occurring in small compartments such as axon terminals that are often invaded by high-frequency Na^+ spikes. This hypothesis led us to quantify the contribution of NCKX to Ca^{2+} clearance in the somata of MNCs, which have low surface-to-volume ratio. To our surprise, no Na^+/Ca^{2+} exchange activity was found in somata. As expected from the absence of NCKX, the Ca^{2+} clearance rates in somata were much slower than in axon

Received July 25, 2003; revised Oct. 24, 2003; accepted Oct. 28, 2003.

This work was supported by a grant from Ministry of Science and Technology (Brain Research Frontier Program). M.-H.K. and S.L. are postgraduate students supported by Program BK21 from the Ministry of Education.

Correspondence should be addressed to Suk-Ho Lee, Department of Physiology, Seoul National University College of Medicine, Chongno-Ku, Yongon-Dong 28, Seoul, 110-799, Korea. E-mail: leesukho@snu.ac.kr.

 0270-6474/03/2311673-08$15.00/0

terminals. We also quantified the contribution of other Ca^{2+} clearance mechanisms in somata, showing that the SERCA pump plays a dominant role. This study is the first clear demonstration of the polarized distribution of Na^{+}/Ca^{2+} exchanger in single neuronal cells.

Materials and Methods

Preparation of isolated nerve endings and brain slice. Isolated nerve endings and brain slices were prepared from male Sprague Dawley rats (11–12 weeks old; 325 ± 25 gm) using previously described methods with small modification (Li and Hatton, 1997; Lee et al., 2002). Briefly, animals were killed by decapitation after being anesthetized with diethyl ether. For isolation of nerve endings, neural lobes were carefully removed from pituitary gland and cut into 9 or 12 pieces with a razor blade in artificial CSF (aCSF). Small pieces of the neural lobe were kept in HEPES-buffered F-10 culture media at room temperature until next use. Just before electrophysiological recording, a piece of neural lobe was transferred to a recording chamber on the stage of an inverted microscope (IX70; Olympus, Tokyo, Japan), in which the neural lobe piece was triturated in culture medium with fire-polished pipettes (300–500 μm in diameter).

For preparation of brain slices, the whole brain was rapidly removed from the skull and chilled in aCSF at 4°C. After trimming a tissue block containing the hypothalamus, coronal brain slices (300-μm-thick) were cut on a vibratome (Vibratome 1000; TPI, St. Louis, MO). Slices were incubated at 37°C for 30 min and thereafter maintained at room temperature (23–25°C) until next use. Supraoptic nuclei were visualized with an upright microscope (BX50WI; Olympus).

Electrophysiological recordings. Calcium currents were evoked from axon terminals or somata of MNCs by conventional whole-cell patch clamp technique. Patch pipettes with a resistance of 5–6 and 2–3 MΩ were used for recording from axon terminals and somata, respectively. The pipette solution contained (in mM): 140 K-gluconate, 5 KCl, 15 HEPES, 4 MgATP, and 4 Na-ascorbate with the pH adjusted to 7.3 with KOH. For measurement of Ca^{2+}-binding ratios in axon terminals, we used Cs^{+}-based pipette solution, which contained 130 Cs-aspartate, 10 TEA-Cl, 5 CsCl, 15 HEPES, 4 MgATP, and 4 Na-ascorbate, pH 7.3 with CsOH. Bath solution for axon terminals contained (in mM): 150 NaCl, 5.4 KCl, 0.5 $MgCl_2$, 1.8 $CaCl_2$, 5 HEPES, and 10 glucose, pH 7.4 with NaOH. Bath solution for somata contained (in mM): 125 NaCl, 5 KCl, 25 $NaHCO_3$, 2 $CaCl_2$, 1 $MgCl_2$, 1.25 NaH_2PO_4, 10 glucose, 5 sucrose, and 0.4 Na-ascorbate, pH 7.4 when saturated with carbogen (95% O_2 and 5% CO_2). The superfusion rate and volume of the recording chamber for slices were 1.8 ml/min and 1.2 ml, respectively. Recordings were made in axon terminals with EPC-9 amplifier and somata with EPC-8 amplifier (HEKA, Lambrecht, Germany). Experiments were performed at 35 ± 1°C. All chemicals were obtained from Sigma (St. Louis, MO), except ruthenium red and 5(6)-carboxyeosin diacetate from Fluka (Buchs, Switzerland), Ru360 from Calbiochem (Nottingham, UK), and fura-2 from Molecular Probes (Eugene, OR).

Cytosolic Ca^{2+} measurement. The procedures for cytosolic Ca^{2+} measurement in isolated nerve ending have been described in detail in our recent publication (Lee et al., 2002). Somatic Ca^{2+} concentration was measured using fluorescence imaging. Cells were loaded with fura-2 (pentapotassium salt) via patch electrodes. For fluorescence excitation, we used a polychromatic light source (xenon-lamp based, Polychrome-II; TILL Photonics, Martinsried, Germany), which was coupled into the epi-illumination port of an upright microscope (BX50; Olympus) via a quartz light guide and a UV condenser. Imaging was performed with a 60× water immersion objective (NA, 0.9; LUMPlanFl, Olympus) and an air-cooled slow-scan CCD camera (SensiCam, PCO, Germany). The monochromator and the CCD camera were controlled by a PC and Digidata 1200A (Axon Instruments, Foster City, CA), running a custom-made software programmed with MicroSoft Visual C++ (version 6.0).

Calibration parameters were determined using *in vivo* calibration as described in Lee et al. (2000). The effective dissociation constant of fura-2 (K_{eff}) was calculated from the equation:

$$K_{eff} = [Ca^{2+}] \times (R_{max} - R_{int})/(R_{int} - R_{min}), \quad (1)$$

where $[Ca^{2+}]$ was entered as 328 nM (assuming a dissociation constant (K_d) of BAPTA of 222 nM at pH 7.2). The estimated R_{min}, R_{max}, and K_{eff} (in μM) in somata measured using the upright microscope were typically 0.87, 5.72, and 1.32, respectively. Those in axon terminals measured using the inverted microscope were 0.27, 3.95, and 0.93, respectively. The K_d of fura-2 was calculated as 201 nM from $K_d = K_{eff} \cdot (\alpha + R_{min})/(\alpha + R_{max})$, where α is the isocoefficient (Zhou and Neher, 1993).

For increasing time resolution and minimizing the photobleaching effect, we adopted the single-wavelength protocol (Helmchen et al., 1996; Lee et al., 2000). Images taken at 10 Hz with single wavelength excitation at 380 nm (F_{380}) were preceded and followed by images with excitation at isosbestic wavelengths (360 nm). F_{iso} (isosbestic fluorescence) values were linearly interpolated between points just before and after the period of excitation at 380 nm. The ratio $R = F_{iso}/F_{380}$ was converted to $[Ca^{2+}]$ with the equation:

$$[Ca^{2+}] = K_{eff} \times (R - R_{min})/(R_{max} - R). \quad (2)$$

Ca^{2+} binding ratio. Ca^{2+} binding ratios of endogenous buffers (κ_S) were estimated according to the single compartment model (Neher and Augustine, 1992; Helmchen et al., 1996; Lee et al., 2000). The differential Ca^{2+} binding ratio of a Ca^{2+} buffer, X, is defined as:

$$\kappa_X = \frac{\partial[XCa]}{\partial[Ca^{2+}]_i} = \frac{[X]_T K_{d,X}}{([Ca^{2+}]_i + K_{d,X})^2}, \quad (3)$$

where $[X]_T$ is the total concentration of Ca^{2+} buffer X, and $K_{d,X}$ is the Ca^{2+} dissociation constants of X. Because κ_X was not completely linear in our experiments, we used incremental Ca^{2+} binding ratio κ'_X (Neher and Augustine, 1992), which is defined as:

$$\kappa'_X = \frac{[X]_T K_{d,X}}{\{([Ca^{2+}]_{i,rest} + K_{d,X}) \times ([Ca^{2+}]_{i,peak} + K_{d,X})\}}. \quad (4)$$

The Ca^{2+} clearance rate exerted by a linear Ca^{2+} clearance mechanism from a single compartment can be described as:

$$d(\Delta[Ca^{2+}]_T)/dt = -\gamma \cdot \Delta[Ca^{2+}]_i, \quad (5)$$

where $\Delta[Ca^{2+}]_T$ and $\Delta[Ca^{2+}]_i$ are magnitudes of total and free Ca^{2+} excursion from the basal level, respectively, and γ is a Ca^{2+} clearance rate constant. From the definition of Ca^{2+} binding ratio:

$$d(\Delta[Ca^{2+}]_T)/dt = d(\Delta[Ca^{2+}]_i)/dt \times (1 + \kappa_S + \kappa_B), \quad (6)$$

where κ_B and κ_S are Ca^{2+} binding ratios of the Ca^{2+} indicator dye (fura-2) and endogenous Ca^{2+} buffers, respectively. And thus, Equation 5 can be rewritten in terms of $\Delta[Ca^{2+}]_i$ as:

$$d(\Delta[Ca^{2+}]_i)/dt = \frac{-\gamma \cdot \Delta[Ca^{2+}]_i}{(1 + \kappa_S + \kappa_B)}. \quad (7)$$

Decay phase of a Ca^{2+} transient ($\Delta[Ca^{2+}]_i(t)$) following a pulse of Ca^{2+} influx can be described by the following equations:

$$\Delta[Ca^{2+}]_i(t) = A \cdot \exp(-t/\tau) \quad (8)$$

$$\tau = (1 + \kappa_S + \kappa_B)/\gamma. \quad (9)$$

Since

$$\Delta[Ca^{2+}]_T(0) = Q/(2FV_a) \quad (10)$$

$$\Delta[Ca^{2+}]_T(0) = A \cdot (1 + \kappa_S + \kappa_B), \quad (11)$$

where F is Faraday constant and V_a is volume of distribution in a cell for Ca^{2+} ions, initial amplitude normalized to the total charge carried by Ca^{2+} influx (A/Q) is

$$A/Q = 1\{2FV_a \cdot (1 + \kappa_S + \kappa_B\}. \quad (12)$$

The value for Q can be measured from time integration of Ca^{2+} current evoked by short depolarization pulse. Estimates of the endogenous Ca^{2+}

binding ratio, κ_S, can be obtained from the negative *x*-axis intercepts of plots of τ, A^{-1}, or $(A/Q)^{-1}$ versus κ_B.

Ca^{2+} clearance rate constant. In our previous paper (Lee et al., 2002), to describe the Ca^{2+} clearance power of a cell when Ca^{2+} transients do not show a single exponential decay, we used the instantaneous Ca^{2+} decay rate constant ($\lambda_{t=0}$) at the peak of a Ca^{2+} transient, which is defined as $(-d[Ca^{2+}]_i/dt)_{t=0}/\Delta[Ca^{2+}]_i$. When the Ca^{2+} transient is fitted to the biexponential function, $A_1 \cdot \exp(-\lambda_1 \cdot t) + A_2 \cdot \exp(-\lambda_2 \cdot t)$, $\lambda_{t=0}$ value can be calculated by the following equation:

$$\lambda_{t=0} = (A_1 \cdot \lambda_1 + A_2 \cdot \lambda_2)/(A_1 + A_2)\,. \quad (13)$$

Because the genuine Ca^{2+} clearance power of the cell is represented by $d(\Delta[Ca^{2+}]_T)/dt$ rather than by $d(\Delta[Ca^{2+}]_i)/dt$, we corrected $\lambda_{t=0}$ for endogenous and exogenous Ca^{2+} buffers by using the Equation 9 and obtained the instantaneous Ca^{2+} clearance rate constant at the peak of the Ca^{2+} transient, $\gamma_{t=0}$, as follows:

$$\gamma_{t=0} = \lambda_{t=0} \cdot (1 + \kappa_S + \kappa_B)\,. \quad (14)$$

Please note that the symbol, $\lambda_{t=0}$, corresponds to $\gamma_{t=0}$ in our previous paper (Lee et al., 2002). In the present paper, however, we introduced a new symbol, λ, to distinguish the decay rate constant from the clearance rate constant, γ.

Calculation of relative contribution curve of a clearance mechanism, X, as a function of $\Delta[Ca^{2+}]_i$. We quantified contribution of a clearance mechanism, *X*, to the entire Ca^{2+} clearance at given $\Delta[Ca^{2+}]_i$ level as follows: (1) We calculated $d(\Delta[Ca^{2+}]_T)/dt$ from two Ca^{2+} transients before and after the application of an inhibitor of *X*, and plotted as a function of $\Delta[Ca^{2+}]_i$; (2) Each $d(\Delta[Ca^{2+}]_T)/dt$ plot was fitted with a fourth-order polynomial function; (3) The difference between the polynomial fit ($f_{control}$) to the $d(\Delta[Ca^{2+}]_T)/dt$ curve under control condition and that ($f_{inhibitor}$) in the presence of the inhibitor was regarded as the contribution made by *X*; (4) The relative contribution made by *X* (R_X) to the entire Ca^{2+} removal mechanism was calculated according to the equation:

$$R_X = (f_{control} - f_X)/f_{control}\,, \quad (15)$$

and plotted as a function of $\Delta[Ca^{2+}]_i$ (see Fig. 4, open gray circles for exemplary plots).

Data analysis. Data were analyzed with IgorPro (version 4.1; WaveMetrics, Lake Oswego, OR). Statistical data are expressed as mean ± SEM, and *n* indicates the number of cells studied. The significance of the differences in $\gamma_{t=0}$ or in R_X were evaluated using Student's *t* test with a significance level of 0.01. Because all the plot and analyses were performed as a function of $\Delta[Ca^{2+}]_i$, hereafter $\Delta[Ca^{2+}]_i$ and $[Ca^{2+}]_i$ will be used interchangeably for convenience.

In situ *hybridization and immunohistochemistry.* The procedures for synthesis of riboprobes and *in situ* hybridization have been described in detail in our recent paper (Lee et al., 2002). For immunohistochemistry, male Sprague Dawley rats (11–12 weeks old; 325 ± 25 gm) were perfused transcardially with 40 ml of 0.1 M PBS, followed by 400 ml 4% paraformaldehyde in PBS. The brains and pituitaries were removed and postfixed by immersion in the same fixative for 16 hr at 4°C. Pituitary or tissue blocks containing hypothalamus were cryoprotected in 25% sucrose in PBS at 4°C overnight, then frozen by immersion into prechilled isopentane in liquid nitrogen. For hypothalamus, serial 16-μm-thick coronal sections were cut with cryostat and adhered to gelatin-coated slides. For neurohypophyses, serial transverse 6-μm-thick sections were collected onto gelatin-coated slides. After a rinse with 0.3% Triton X-100 in 0.05 M PBS (PBS-TX), the sections were treated with 1% H_2O_2 in PBS-TX and they were incubated sequentially in (1) 0.5% bovine serum albumin (BSA) in PBS for 1 hr, (2) rabbit anti-NCKX2 antibody (Affinity BioReagents, Golden, CO) diluted 1:100 in 0.5% BSA + PBS-TX for 16 hr at 4°C, (3) a 1:200 dilution of goat biotinylated anti-rabbit IgG (Vector Laboratories, Burlingame, CA) for 90 min, and (4) a 1:100 dilution of avidin biotin peroxidase complex (ABC Vectastain; Vector Laboratories) for 90 min. NCKX2-positive signals were visualized with diaminobenzidine tetrahydrochloride (Sigma) For pituitary gland, sections were coverslipped after counterstaining with cresyl violet (Sigma). Then slides were analyzed and photographed using BX50F3 upright microscope (Olympus) equipped with a Progres C14 digital camera (Jenoptik, Jena, Germany).

Results

We investigated the Ca^{2+} clearance mechanisms in the somata and axon terminals of supraoptic MNCs by analyzing the decay phases of Ca^{2+} transients evoked in response to depolarizing pulses. Because the decay rate of free Ca^{2+} ($-d[Ca^{2+}]_i/dt$) is affected not only by Ca^{2+} clearance mechanisms but also by the concentrations of endogenous and exogenous Ca^{2+} buffers, we first estimated the endogenous Ca^{2+} binding ratios (κ_S) in two loci. Using these values, we converted $-d[Ca^{2+}]_i/dt$ into the Ca^{2+} clearance rate ($-d[Ca^{2+}]_T/dt$), which represents the genuine power of Ca^{2+} clearance mechanisms in the cell.

Endogenous Ca^{2+} binding ratios in axon terminals and somata of MNCs

Endogenous Ca^{2+} binding ratios (κ_S) in the axon terminals and somata of MNCs were estimated according to the single compartment model (Neher and Augustine, 1992). To evoke Ca^{2+} transients, we used depolarizing pulses of relatively short duration (from −60 to 0 mV; 20 msec for somata, 30 msec for axon terminals). Under these conditions, the initial amplitudes of Ca^{2+} transients were lower than 200 nM, and Ca^{2+} transients were well fitted by monoexponential functions.

Somata of MNCs were loaded with an internal solution containing 250 μM fura-2. Time course of fura-2 loading within the soma of the MNC is shown in Figure 1*Aa* (open circles). After the break-in, Ca^{2+} transients were evoked every 1 min. Ca^{2+} transients measured at various fura-2 were depicted near the fura-2 loading trace. As cytosolic fura-2 concentration increased, amplitudes and decay rates of Ca^{2+} transients decreased. To estimate κ_S in the somata of MNCs, time constants (Fig. 1*Ab*, open circles, left ordinate) and inverse of amplitudes (Fig. 1*Ab*, filled gray circles, right ordinate) were plotted against the incremental Ca^{2+} binding ratio of fura-2 (κ'_B). The κ_S values obtained using Equations 9 and 11 were 79 ± 2.6 ($n = 8$) and 63 ± 5 ($n = 8$), respectively, showing no significant difference. As the single compartment model predicts, $A\tau$ showed no significant dependence on κ'_B (Fig. 1*Ab*, inset).

When axon terminals were loaded with 250 μM fura-2, there were negligible effects of the exogenous buffer on Ca^{2+} transients, indicating that 250 μM fura-2 is not sufficient to compete with endogenous buffers. We therefore increased the fura-2 concentration to 500 μM. The time course of fura-2 loading into the axon terminal is shown in Figure 1*Ba*. Shortly after the break-in, Ca^{2+} currents were evoked by depolarizing pulses. The method to estimate κ_S in the soma was similar to that used in axon terminals, except that the initial amplitude of each Ca^{2+} transient (A) was normalized to the total charge of corresponding Ca^{2+} influx (Q) to compensate for the error caused by rundown of Ca^{2+} current (Fig. 1*Ba*, inset). For this purpose, we used a Cs^+-based pipette solution. As shown in Figure 1*Bb*, τ and $(A/Q)^{-1}$ were plotted against κ'_B, and κ_S was calculated according to Equations 9 and 12. Mean values for κ_S estimates from analyses of τ and $(A/Q)^{-1}$ were 179 ± 35 ($n = 3$) and 187 ± 19 ($n = 3$), respec-

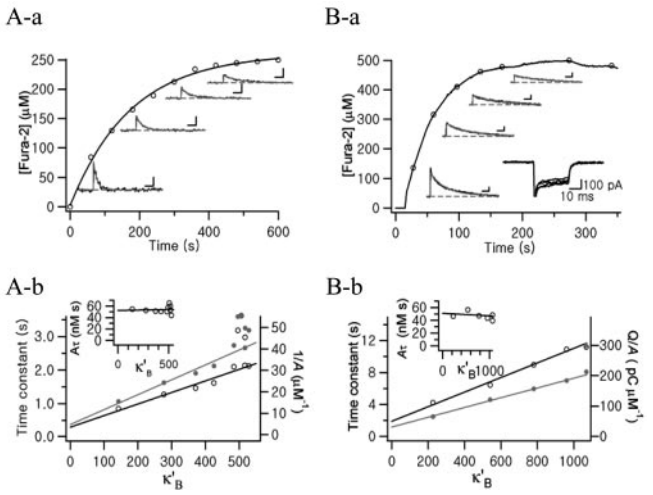

Figure 1. Representative examples for estimation of endogenous Ca^{2+} binding ratios (κ_S) in the soma of a MNC (*A*) and in the neurohypophysial axon terminal (*B*). *Aa*, Time course of fura-2 (250 μM) loading during whole-cell patch recording (abscissa: elapsed time after break-in). Fura-2 concentration was calculated from isosbestic fluorescence averaged from ROI drawn on the soma. Exponential fit to the loading curve was superimposed ($\tau = 175.8$ sec). After break-in, Ca^{2+} transients were evoked every 1 min by depolarizing pulses from −60 to 0 mV (20 msec duration). Four exemplar Ca^{2+} transients are shown along the fura-2 loading curve. Calibration: 2 sec, 20 nM. Monoexponential functions were fitted to the decay phases of four Ca^{2+} transients ($\tau = 1273.7$, 1615.9, 2138.2, and 2973.3 msec, from left to right). *Ab*, Plots of time constants (open circles, left ordinate) and inverse of initial amplitudes (1/*A*; gray filled circles, right ordinate) versus incremental Ca^{2+} binding ratio of fura-2 (κ'_B). κ_S were estimated from *x*-axis intercepts of regression lines. The plot of $A\tau$ versus κ'_B (inset) shows no significance dependence on κ'_B. *Ba*, Time course of fura-2 (500 μM) loading in the NHP axon terminal. Ca^{2+} transients were evoked by depolarizing pulses (30 msec duration) during whole-cell patch recording. Four exemplar Ca^{2+} transients (calibration: 2 sec, 20 nM) are shown, and their decay phases were well fitted by exponential functions whose τ values are 4225.2, 6426.9, 8970.7, and 1089.6 msec. *Bb*, Plots of time constants (open circles, left ordinate) and inverse of normalized amplitudes (gray filled circles, right ordinate) versus κ'_B. Inset, Plot of $A\tau$ versus κ'_B.

tively. These values are not substantially different from the value reported by Stuenkel (1994) (174 ± 17.6) in the same preparation. These results indicate that the endogenous Ca^{2+} binding ratio is significantly higher in the axon terminals than in the somata of MNCs ($p < 0.01$ by Student's *t* test).

Ca^{2+} clearance in somata and axon terminals of MNCs

To investigate Ca^{2+} clearance mechanisms in the axon terminals and somata of MNCs, Ca^{2+} transients were evoked by depolarizing pulses, the durations of which were adjusted such that the peak $[Ca^{2+}]$ fell within the range 1.0 ± 0.2 μM (typically, 200 msec in axon terminals and 300 msec in somata). To avoid inhibition of K^+-dependent Na^+/Ca^{2+} exchange activity, we used a K^+-rich pipette solution containing 50 μM fura-2 (Lee et al., 2002). The Ca^{2+} transients were recorded from the soma (Fig. 2*Ba*, black line) and the axon terminal (Fig. 2*Bb*, black line) under control condition. From decay phases of these Ca^{2+} transients, we calculated values for $-d[Ca^{2+}]_i/dt$ and plotted them as a function of $\Delta[Ca^{2+}]_i$ (Fig. 2*B*, insets). These results indicated that $-d[Ca^{2+}]_i/dt$ is faster in the axon terminal than in the soma. To take into account the difference in κ_S in the two loci, $-d[Ca^{2+}]_i/dt$ was converted into $-d[Ca^{2+}]_T/dt$ according to Equation 6 (Fig. 2*C*; rectangles, soma; circles, axon terminal). Estimates for $\gamma_{t=0}$, which represents the Ca^{2+} clearance power of a cell at the peak of Ca^{2+} transient, were obtained from the corresponding $\lambda_{t=0}$ according to Equation 14. The mean values for

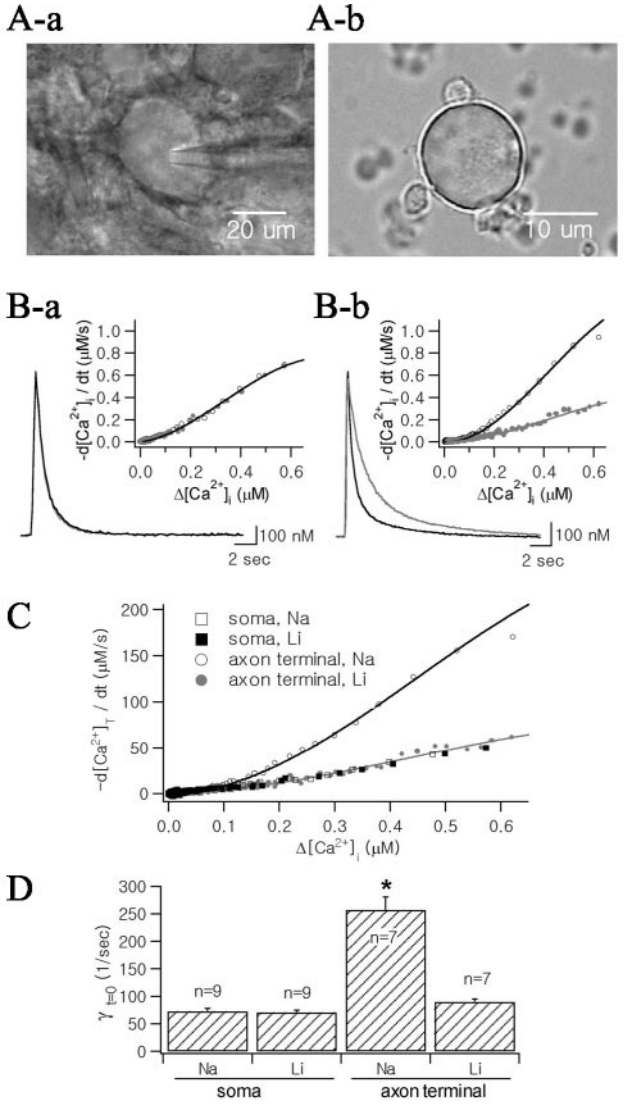

Figure 2. Effects of external Na^+ reduction (replaced with Li^+) on Ca^{2+} transients of somata and axon terminals. *A*, Micrograph of the MNC soma in supraoptic nucleus (*Aa*) and that of axon terminals dissociated from neurohypophysis (*Ab*). *Ba*, Two Ca^{2+} transients from the soma were superimposed in control condition (black line) and after the 10 min superfusion with low Na^+ aCSF (24 mM, gray line). K^+ pipette solution containing 50 μM fura-2 was used for the internal solution. Ca^{2+} transients were evoked by depolarizing pulses (from −60 to 0 mV; 300 msec duration). *Bb*, Two Ca^{2+} transients recorded in the axon terminal (black line: control; gray line: low Na^+ condition). The same internal solution was used as *Ba*. Ca^{2+} transients were evoked by 200 msec depolarization. Insets, Time derivatives of decay phases of Ca^{2+} transients ($-d[Ca^{2+}]_i/dt$) were plotted as a function of $\Delta[Ca^{2+}]_i$, and fitted with fourth-order polynomial equations (open circles and black lines: control condition, filled circles and gray lines: low Na+ condition). *C*, Time derivatives of total Ca^{2+} ($d[Ca^{2+}]_T/dt$) decay as a function of $\Delta[Ca^{2+}]$, which were obtained from Ca^{2+} transients illustrated in *B*. Four plots obtained from the soma (rectangles) and the axon terminal (circles) were superimposed. Values for $d[Ca^{2+}]_T/dt$ were calculated according to Equation 6, assuming that κ_S values for soma and axon terminal are 79 and 187, respectively, and that K_D of fura-2 is 201 nM. Plots of $-d[Ca^{2+}]_T/dt$ were fitted with fourth-order polynomial equations. *D*, Mean values for instantaneous Ca^{2+} clearance rate constants ($\gamma_{t=0}$) calculated using Equation 14 before (indicated by "Na") and after extracellular Na^+ reduction (indicated by "Li"). Asterisk indicates statistical significance ($p < 0.01$).

$\gamma_{t=0}$ in somata and axon terminals were 81.3 ± 5.0 sec^{-1} ($n = 9$) and 250.3 ± 23.5 sec^{-1} ($n = 7$), respectively (Fig. 2*D*), indicating that Ca^{2+} clearance power is about threefold larger in axon terminals than in somata.

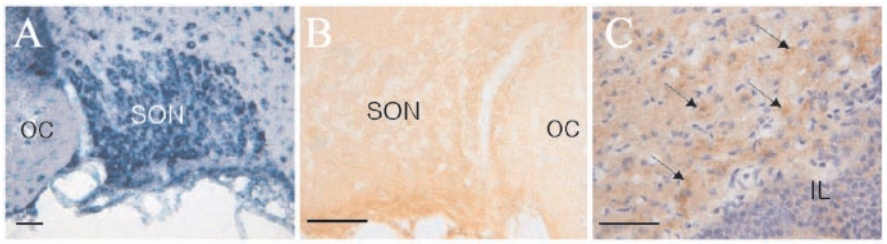

Figure 3. Expression of NCKX2 or its transcripts in the supraoptic nucleus (SON) and the neurohypophysis. In SON, positive signals for NCKX transcripts were revealed by *in situ* hybridization (*A*). NCKX2 mRNA was detected using digoxigenin-labeled NCKX2 antisense riboprobes. Somata of MNCs were strongly positive to NCKX2. However, the micrograph obtained from immunohistochemistry indicates that NCKX2-immunoreactive signals are very weak in SON (*B*). In neurohypophysis, intense NCKX2-immunoreactive signals were localized in numerous Herring bodies (*C*, arrows). Note the difference in staining density between *B* and *C*. IL, Intermediate lobe; OC, optic chiasm; SON, supraoptic nucleus. Scale bars, 50 μm.

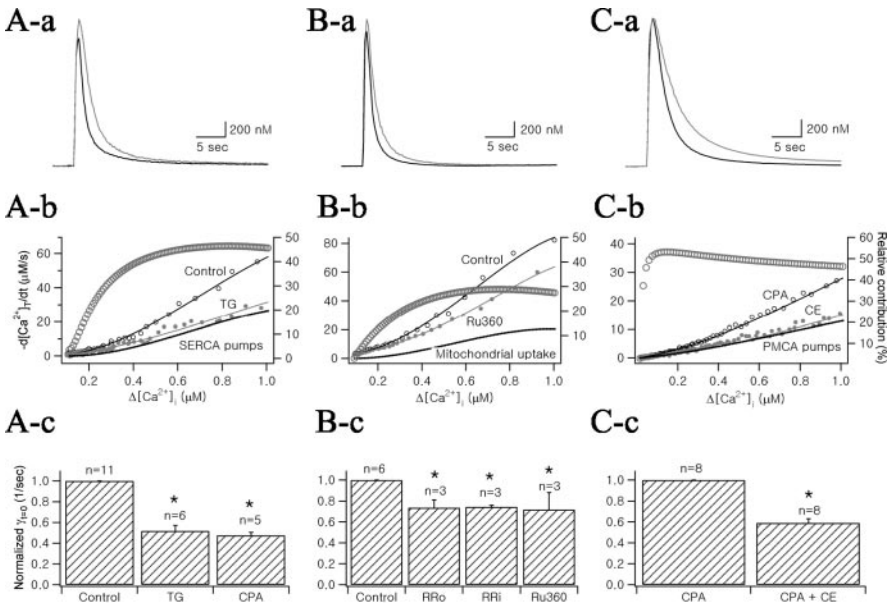

Figure 4. Effects of specific inhibitors of SERCA pumps, mitochondria, and PMCA pumps on Ca^{2+} transients of MNCs somata. *Aa*, Two Ca^{2+} transients evoked in control condition (black line) and in the presence of 1 μM thapsigargin (gray line) were superimposed. *Ab*, Plots of total Ca^{2+} decay rate ($-d[Ca^{2+}]_T/dt$) as a function of $\Delta[Ca^{2+}]_i$, which were obtained from decay phases of two Ca^{2+} transients in A*a* according to Equation 6. Fourth-order polynomial fits were superimposed on the plots (continuous lines). The difference between two polynomial fits to $-d[Ca^{2+}]_T/dt$ curves was plotted as a dotted line (marked by "SERCA pumps"). Relative contribution of SERCA to Ca^{2+} clearance (R_{SERCA}) was calculated according to the Equation 15 and plotted as a function of $\Delta[Ca^{2+}]_i$ (gray open circles, right ordinate). *Ac*, Bar graph representing mean values for $\gamma_{t=0}$ normalized to the control condition. TG, Thapsigargin; CPA, cyclopiazonic acid (10 μM). *Ba*, Two Ca^{2+} transients in the control condition (black line) and in the presence of 10 μM Ru360 (gray line) were superimposed. *Bb*, $-d[Ca^{2+}]_T/dt$ and $R_{Mitochondria}$ were plotted by the similar procedure as in *Ab*. *Bc*, Normalized mean values for $\gamma_{t=0}$ of Ca^{2+} transients in conditions indicated below the abscissa. RRo, Extracellular application of 20 μM ruthenium red; RRi, intracellular application of 10 μM ruthenium red. *Ca*, Superimposed Ca^{2+} transients recorded in the presence of CPA (black line) and CE (gray line). *Cb*, $-d[Ca^{2+}]_T/dt$ and R_{PMCA} were plotted by similar procedure with *Ab*. *Cc*, Normalized mean values for $\gamma_{t=0}$ averaged from eight cells in control condition, in the presence of CPA, and in the presence of CPA and CE were summarized.

Na^+/Ca^{2+} exchange contributes little to Ca^{2+} clearance in somata of MNCs

To investigate the contribution of Na^+/Ca^{2+} exchange to Ca^{2+} clearance, the effect of reducing extracellular $[Na^+]$ (replacement of the 125 mM NaCl in the bathing solution with equimolar LiCl) on Ca^{2+} clearance rates was determined in the somata of MNCs and in NHP axon terminals. In somata of MNCs, Ca^{2+} transients in control condition (black line) were compared with those observed 10 min after superfusion with low Na^+ aCSF (gray line). The two Ca^{2+} transients could be almost completely superimposed (Fig. 2*Aa*), indicating that removal of external Na^+ had no effect on Ca^{2+} transients. In eight other cells, no change in Ca^{2+} transients was observed at least 10 min after superfusion with low Na^+-aCSF. The mean value for $\gamma_{t=0}$ after reduction of extracellular Na^+ (81.3 ± 5.0 sec^{-1}; $n = 9$) was not significantly different from that under control conditions ($p = 0.27$, by Student's t test for paired samples) (Fig. 2*C*). In contrast, the decay phases of Ca^{2+} transients in NHP axon terminals were significantly slowed by reduction of extracellular Na^+ to 20 mM (Fig. 2*Bb*), consistent with our previous report (Lee et al., 2002). The mean values for $\gamma_{t=0}$ before and after reduction of extracellular Na^+ were 250.3 ± 23.5 sec^{-1} and 87.5 ± 5.1 sec^{-1}, respectively ($n = 7$; $p < 0.01$) (Fig. 2*D*).

In Figure 2*C*, plots of $-d[Ca^{2+}]_T/dt$ as a function of $[Ca^{2+}]_i$ obtained from the soma (rectangles) and the axon terminal (circles) under conditions of normal (open symbols) and low $[Na^+]$ (closed symbols) were superimposed. The $-d[Ca^{2+}]_T/dt$ plot of the axon terminal under low Na^+ condition overlapped almost completely with that of the soma under normal Na^+ conditions, indicating that the Ca^{2+} clearance power of the axon terminal in the absence of Na^+/Ca^{2+} exchange is equivalent to that of the soma. This finding was confirmed by results for $\gamma_{t=0}$ under each condition (Fig. 2*D*). Above results suggest that greater Ca^{2+} clearance power in axon terminals than in somata can be attributed to Na^+/Ca^{2+} exchanger and that Ca^{2+} clearance in the somata is mediated by mechanisms other than Na^+/Ca^{2+} exchange.

NCKX2 is highly localized to axon terminals

To test whether the polarization of Na^+/Ca^{2+} exchange activity in axon terminals is caused by the specific localization of Na^+/Ca^{2+} exchange proteins, we performed immunohistochemistry in SON and in NHP. Because we showed in our previous report (Lee et al., 2002) using *in situ* hybridization technique that NCKX2 is a major isoform of NCKX present in SON (Fig. 3*A*), the expression of NCKX2 was examined.

The location of SON was confirmed by the adjacent optic chiasm. NHP was distinguished from the adjacent intermediate lobe of the hypophysis by the lower density of nuclei that were counterstained with cresyl violet. NCKX2-positive signals were visualized with diaminobenzidine tetrahydrochloride as brown color. Although there were few NCKX2-positive signals in SON (Fig. 3*B*), intense staining for NCKX2 was observed in NHP, in a form resembling Herring bodies (Fig. 3*C*, arrows).

Other Ca^{2+} clearance mechanisms in somata of MNCs

Because Na^+/Ca^{2+} exchange contributed little to Ca^{2+} clearance in the somata of MNCs, we investigated the contribution of other putative Ca^{2+} clearance mechanisms: SERCA, mitochondrial Ca^{2+} uniporter, and PMCA.

To study the contribution of SERCA pumps to Ca^{2+} clearance, we examined the effects of thapsigargin (TG; 1 μM) and cyclopiazonic acid (CPA; 10 μM), specific inhibitors of the SERCA pump, to the decay phase of Ca^{2+} transients. Because the effects induced by these inhibitors depend on the incubation time (Sagara et al., 1992), we superfused the slice with SERCA pump inhibitors ~10 min before estimating their effects. Figure 4*Aa* illustrates representative Ca^{2+} transients before and after the addition of 1 μM TG to the extracellular solution. The Ca^{2+} decay rate was significantly slowed down by TG.

The contribution of mitochondrial Ca^{2+} uptake was measured using Ru360 and ruthenium red, blockers of mitochondrial Ca^{2+} uniporters. The superfusion of 10 μM Ru360 for 30 min caused a slowing of Ca^{2+} decay (Fig. 4*Ba*). Extracellular perfusion of 20 μM ruthenium red and intracellular application of 10 μM ruthenium red showed similar effects as Ru360.

The role of PMCA pumps in Ca^{2+} clearance was tested using 5(6)-carboxyeosin diacetate (CE). It was reported that CE can inhibit SERCA pumps as well as PMCA pumps (Fierro et al., 1998). To assess the role of PMCA pumps by using CE, SERCA pumps were inhibited by 10 μM CPA or 1 μM thapsigargin before the addition of CE. Comparison of two Ca^{2+} transients in the presence of CPA (control condition) and 13 min after additional application of CE (40 μM) revealed that CE slowed the Ca^{2+} decay phase (Fig. 4*Ca*). Because CPA or thapsigargin was present in the extracellular perfusion solutions throughout the experiment, it is likely that CE-induced decrease in Ca^{2+} decay rate is caused by PMCA inhibition.

We calculated $-d[Ca^{2+}]_T/dt$ and $\gamma_{t=0}$ from the Ca^{2+} transients before and after the application of each blocker, as described in Figure 2. The relative contribution of each mechanism to Ca^{2+} clearance over the whole range of $[Ca^{2+}]_i$ was calculated from $-d[Ca^{2+}]_T/dt$ using Equation 15, and is shown as open circles superimposed onto each $-d[Ca^{2+}]_T/dt$ plot (right ordinates; see Materials and Methods for details). We found that R_{SERCA} increased as $[Ca^{2+}]_i$ increased, reaching its maximal value (46.4%) (Fig. 4*Ab*). R_{SERCA} calculated according to the equation $(\gamma_{t=0,control} - \gamma_{t=0,TG})/\gamma_{t=0,control}$ was 47.6%. A similar value was obtained when R_{SERCA} was calculated from $\gamma_{t=0}$ in the presence of CPA ($\gamma_{t=0,CPA}$). TG decreased $\gamma_{t=0}$ by 48.2 ± 5.4% ($n = 6$) and CPA decreased by 52.3 ± 2.6% ($n = 5$), with no significant difference observed between these two agents ($p = 0.54$) (Fig. 4*Ac*). $R_{Mitochondria}$ obtained from the Ru360 results showed an increase as $[Ca^{2+}]_i$ increased until it reached a maximum value (28.6%) (Fig. 4*Bb*). The decreases in $\gamma_{t=0}$ induced by Ru360 and by extracellular and intracellular ruthenium red were 28.2 ± 16.2% ($n = 6$), 26.4 ± 7.5% ($n = 3$), and 25.5 ± 1.4% ($n = 3$), respectively (Fig. 4*Bc*). The relative contribution of PMCA (R_{PMCA}) was characteristic in that R_{PMCA} steeply increased and reached a maximal value at a lower $[Ca^{2+}]_i$ range than the other Ca^{2+} clearance mechanisms (Fig. 4*Cb*). After reaching the maximal value, R_{PMCA} decreased as $[Ca^{2+}]_i$ increased. In the presence of CPA where $\gamma_{t=0}$ was 47.6% of the control value, CE-induced decrease in $\gamma_{t=0}$ was 41.0 ± 3.96% ($n = 8$), indicating that the decrease in $\gamma_{t=0}$ that can be ascribed to CE-induced PMCA inhibition is 19.5%.

Figure 5*A* summarizes the relative contribution of each mechanism to somatic Ca^{2+} clearance at a given $[Ca^{2+}]_i$ range. Because the experiments of PMCA inhibition were performed in the presence of SERCA pump inhibitors, R_{PMCA} was corrected for normal conditions. After reaching the maximal value at relatively low $[Ca^{2+}]_i$ range, R_{PMCA} steeply decreased. In contrast, R_{SERCA} and $R_{Mitochondria}$ increased as $[Ca^{2+}]_i$ increased, reaching their maximum contributions. This can be interpreted as a transition of the major Ca^{2+} clearance mechanism from a low-capacity, high-affinity mechanism to high-capacity, low-affinity mechanisms as $[Ca^{2+}]_i$ increases. In Figure 5*B*, the relative contributions of each Ca^{2+} clearance mechanism calculated using $\gamma_{t=0}$ value were summarized. Mean values of the relative contribution of SERCA pumps, mitochondrial uptake, and PMCA pumps were 47.8 ± 7.2% ($n = 9$), 27.4 ± 6.9% ($n = 6$), and 21.1 ± 4.5% ($n = 8$), respectively. By taking the sum of these three mechanisms, we could account for >90% of Ca^{2+} clearance. This result is consistent with the finding that contribution of Na^+/Ca^{2+} exchange to Ca^{2+} clearance in the somata of MNCs is negligible (Fig. 2).

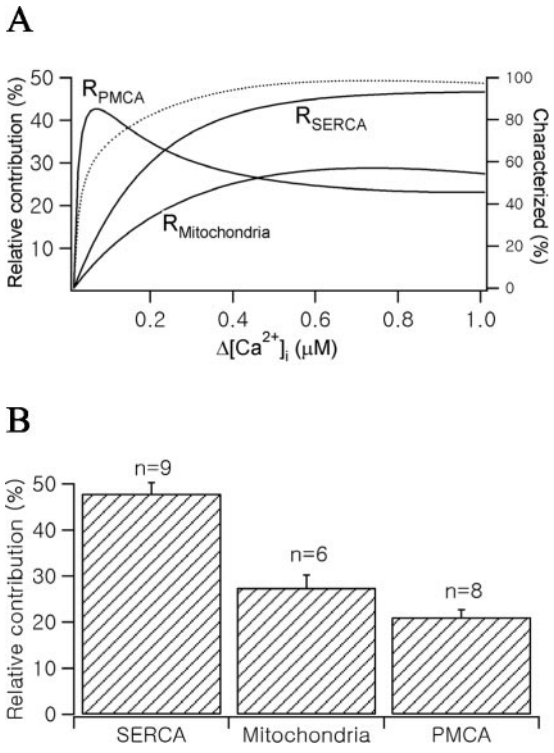

Figure 5. Relative contribution of Ca^{2+} clearance mechanisms in MNCs somata. *A*, R_{SERCA}, $R_{Mitochondria}$, and R_{PMCA} shown in Figure 4*Ab*, *Bb*, and *Cb* were summarized (left ordinate). R_{PMCA} was corrected for the condition in the absence of CPA. The dotted line represents a characterized fraction of total Ca^{2+} clearance rate (right ordinate). *B*, The bar graph represents relative contribution of each Ca^{2+} clearance mechanism calculated from $\gamma_{t=0}$ values.

Discussion

Although recent studies increased our understanding of differences in Ca^{2+} regulation mechanisms among neuronal cell types, little is known about the differences in Ca^{2+} regulation mechanisms in different parts of a single neuron. We have previously shown that, in axon terminals of rat neurohypophyses, the K^+-dependent Na^+/Ca^{2+} exchanger, NCKX, plays a dominant role, accounting for ~60% of the total Ca^{2+} clearance (Lee et al., 2002). In the present study, we investigated the differences in Ca^{2+} regulation mechanisms between axon terminals and somata of MNCs and found that the two compartments of MNCs clear Ca^{2+} loads in different ways: (1) the endogenous Ca^{2+}

binding ratio (κ_S) and Ca^{2+} clearance rate constant ($\gamma_{t=0}$) in axon terminals were significantly higher than in somata of MNCs; (2) the distribution of NCKX is polarized to axon terminals; (3) sequestration of Ca^{2+} via SERCA pumps is a major Ca^{2+} clearance mechanism in the somata of MNCs. These results indicate that the two compartments of MNCs clear Ca^{2+} loads in different ways, and that the higher Ca^{2+} clearance power in axon terminals is caused by the polarized distribution of NCKX.

Subcellular localization of Na^+/Ca^{2+} exchangers in neurons

Two different families of Na^+/Ca^{2+} exchangers, NCX and NCKX, are expressed in various regions of the brain. Three different genes for NCX isoforms and four different genes for NCKX isoforms have been cloned (Nicoll et al., 1990, 1996; Li et al., 1994; Tsoi et al., 1998; Kraev et al., 2001; Li et al., 2002). Distributions of each gene in various regions of the brain have been studied by *in situ* hybridization. Apart from NCKX1, which has the most restricted tissue distribution, being found only in retinal photoreceptor (Prinsen et al., 2000), transcripts for the other NCKX isoforms and for all NCX isoforms are widely distributed throughout the brain (Tsoi et al., 1998; Kraev et al., 2001; Lee et al., 2002; Li et al., 2002).

However, information on the subcellular localization of Na^+/Ca^{2+} exchangers is very limited. In cultured hippocampal neurons (Reuter and Porzig, 1995; Canitano et al., 2002) and the ciliary ganglia of the chick (Juhaszova et al., 2000), immunocytochemical studies have shown the preferential localization of NCX to presynaptic nerve terminals. Immunogold electron microscopy in rat brain section, however, revealed that NCX1 is localized to both the presynaptic and the postsynaptic sites of excitatory synapses (Canitano et al., 2002). Functional studies can also be useful in demonstrating the expression and the role of Na^+/Ca^{2+} exchangers. Slowing of Ca^{2+} decay by removal of Na^+ has been observed in the somata of some neurons (Mironov et al., 1993; Fierro et al., 1998). Changes in $[Ca^{2+}]_i$ in presynaptic nerve terminals can be indirectly monitored by measuring miniature IPSCs (mIPSCs). In acutely isolated neurons containing functional GABAergic presynaptic boutons, a transient increase in mIPSCs was induced by removal of external Na^+ in the presence of ouabain, suggesting the presence of NCX in these nerve terminals (Doi et al., 2002). Flux studies using synaptosomal preparations have shown that the efflux of radiolabeled Ca^{2+} could be attenuated by removal of external Na^+ and accelerated by reintroduction of external Na^+ (Sanchez-Armass and Blaustein, 1987).

Although these results are thought to represent the contribution of NCX, the possible contribution of NCKX cannot be excluded because these studies were not designed to distinguish between their activities. In the present study, however, we performed functional tests together with immunocytochemical assays, and we found that NCKX does not function in the somata but is localized specifically to axon terminals of supraoptic MNC neurons. To our knowledge, our studies are the first to demonstrate the subcellular localization of a specific Ca^{2+} regulation mechanism in different parts of a single neuron. We cannot yet state whether the specific localization of NCKX to axon terminals is specific to supraoptic MNC neurons or generally found in other regions. It also needs to be investigated in future studies whether the localization and role of NCKX are distinguished from those of NCX or overlap with each other.

Ca^{2+} clearance mechanisms in the somata of MNCs

Neuronal cells clear Ca^{2+} loads by extrusion across the plasma membrane or by sequestration into intracellular organelles. In the present study, we characterized the relative contribution of Ca^{2+} clearance mechanisms in the somata of MNCs using pharmacological and ion substitution methods, showing that sequestration of Ca^{2+} into the ER via SERCA pumps is the dominant form of Ca^{2+} removal. ER is capable of rapidly sequestering Ca^{2+} and functions as a major Ca^{2+} clearance mechanism in dendrites and the somata of some neurons (Markram et al., 1995; Fierro et al., 1998). The presence of SERCA pumps in somata of MNCs was previously suggested by the finding that SERCA pump inhibitors prevented the generation of depolarizing afterpotentials and phasic firing activity (Li and Hatton, 1997).

Recently, the role of mitochondria in cytosolic Ca^{2+} handling has been investigated in various cell types. In adrenal chromaffin cells, mitochondrial Ca^{2+} uptake has been shown to play a major role in Ca^{2+} clearance (Herrington et al., 1996; Park et al., 1996). In addition to directly taking up cytosolic Ca^{2+} via Ca^{2+} uniporters, mitochondria contribute to Ca^{2+} clearance indirectly by providing fuel to ATP-dependent Ca^{2+} pumps. In synaptic terminals of retinal bipolar neurons, mitochondria have been shown to contribute to Ca^{2+} clearance primarily as an energy source for other clearance mechanisms, and mitochondrial Ca^{2+} uptake was observed only when PMCA pump, which is the major form of Ca^{2+} clearance in this tissue, was inhibited (Zenisek and Matthews, 2000). In somata of neurons, however, contributions of mitochondria to Ca^{2+} clearance has not been investigated.

For investigating mitochondrial functions, the protonophore carbonyl cyanide *m*-chlorophenylhydrazone (CCCP) has been frequently used as a mitochondrial inhibitor. Because protonophores dissipate transmembrane potential of intracellular organelles including mitochondria, many cytotoxic materials including Ca^{2+} can be released from them. These nonspecific effects make protonophores not useful for assaying the role of mitochondria in Ca^{2+} clearance. We found that bath application of CCCP significantly increased resting $[Ca^{2+}]$ in the somata of MNCs (data not shown). The increase of resting $[Ca^{2+}]$ by CCCP was observed in the absence of extracellular Ca^{2+}, suggesting that it was released from intracellular stores. Thus, we investigated the mitochondrial contribution to Ca^{2+} clearance using specific inhibitors of mitochondrial Ca^{2+} uniporters. Application of ruthenium red and Ru360 had no effect on resting Ca^{2+} concentration, although they slightly decreased peak Ca^{2+} amplitude. The Ca^{2+} decay rate measured in the presence of ruthenium red did not differ from that measured in the presence of Ru360 ($p = 0.92$; Student's *t* test). These findings suggest that the direct contribution of mitochondria to Ca^{2+} clearance, by taking up cytosolic Ca^{2+} via Ca^{2+} uniporters, accounts for ~25% of the total clearance in the somata of MNCs.

Physiological implications

Because secretion of vasopressin and oxytocin is accompanied by AP bursts in MNCs (15–20 Hz; Cazalis et al., 1985), somata and axon terminals frequently undergo large Ca^{2+} loads in physiological conditions. When we mimicked the burst spikes by applying a train of 3 msec depolarization pulses at a frequency of 15 Hz for 5 sec, the increase in $[Ca^{2+}]_i$ was similar to that evoked by a depolarizing pulse from −60 to 0 mV for 300 msec, as used in the present study. Thus, SERCA pumps and NCKX, which are low-affinity, high-capacity Ca^{2+} clearance mechanisms in somata and axon terminals, respectively, might play a dominant role in

Ca^{2+} clearance at the physiological range of Ca^{2+} loads associated with peptide hormone secretion.

The results of the present study indicate that the axon terminals and somata of MNCs clear Ca^{2+} loads in different ways. Extrusion of Ca^{2+} across the plasma membrane via K^+-dependent Na^+/Ca^{2+} exchange accounts for >60% of Ca^{2+} clearance in axon terminals, whereas sequestration of Ca^{2+} into the ER via SERCA pumps is the dominant Ca^{2+} clearance mechanism in the somata of MNCs. Including mitochondrial Ca^{2+} uptake, >70% of Ca^{2+} clearance is mediated by sequestration of Ca^{2+} into the intracellular organelles in the somata of MNCs. Why axon terminals and somata of MNCs adopt different Ca^{2+} clearance mechanisms? The differences in κ_S and surface-to-volume ratio between two compartments may provide a possible explanation. Because the Ca^{2+} decay rate constant is inversely proportional to κ_S, axon terminals require higher Ca^{2+} clearance power to attain a similar Ca^{2+} decay rate as somata. This requirement may be met by localized expression of NCKX2 in NHP axon terminals. The diameters of axon terminals of MNCs range from 2 to 15 μm, whereas those of somata range from 30 to 50 μm. Because axon terminals have higher surface-to-volume ratio, extrusion of Ca^{2+} across the plasma membrane can be the most effective mechanism for Ca^{2+} clearance. In contrast to axon terminals, extrusion across the plasma membrane may not be very effective in clearing Ca^{2+} from the somata of MNCs because of low surface-to-volume ratio. Thus, using intracellular stores seems to be a good strategy for overcoming low surface-to-volume ratio.

References

Billups B, Forsythe ID (2002) Presynaptic mitochondrial calcium sequestration influences transmission at mammalian central synapses. J Neurosci 22:5840–5847.

Canitano A, Papa M, Boscia F, Castaldo P, Sellitti S, Taglialatela M, Annunziato L (2002) Brain distribution of the Na^+/Ca^{2+} exchanger-encoding genes NCX1, NCX2, and NCX3 and their related proteins in the central nervous system. Ann NY Acad Sci 976:394–404.

Cazalis M, Dayanithi G, Nordmann JJ (1985) The role of patterned burst and interburst interval on the excitation-coupling mechanism in the isolated rat neural lobe. J Physiol (Lond) 369:45–60.

Cervetto L, Lagnado L, Perry RJ, Robinson DW, McNaughton PA (1989) Extrusion of calcium from rod outer segments is driven by both sodium and potassium gradients. Nature 337:740–743.

Doi A, Kakazu Y, Akaike N (2002) Na^+/Ca^{2+} exchanger in GABAergic presynaptic boutons of rat central neurons. J Neurophysiol 87:1694–1702.

Fierro L, Dipolo R, Larno I (1998) Intracellular calcium clearance in purkinje cell somata from rat cerebellar slices. J Physiol (Lond) 510:499–512.

Helmchen F, Imoto K, Sarkmann B (1996) Ca^{2+} buffering and action potential-evoked Ca^{2+} signaling in dendrites of pyramidal neurons. Biophys J 70:1069–1081.

Herrington J, Park YB, Bobcock DF, Hille B (1996) Dominant role of mitochondria in clearance of large Ca^{2+} loads from rat adrenal chromaffin cells. Neuron 16:219–228.

Juhaszova M, Church P, Blaustein MP, Stanley EF (2000) Location of calcium transporters at presynaptic terminals. Eur J Neurosci 12:839–846.

Kraev A, Quednau BD, Leach S, Li XF, Dong H, Winkfein R, Perizzolo M, Cai X, Yang R, Philipson KD, Lytton J (2001) Molecular cloning of a third member of the potassium-dependent sodium-calcium exchanger gene family, NCKX3. J Biol Chem 276:23161–23172.

Lee SH, Rosenmund C, Schwaller B, Neher E (2000) Differences in Ca^{2+} buffering properties between excitatory and inhibitory hippocampal neurons from the rat. J Physiol (Lond) 525 :405–418.

Lee SH, Kim MH, Park KH, Earm YE, Ho WK (2002) K^+-dependent Na^+/Ca^{2+} exchange is a major Ca^{2+} clearance mechanism in axon terminals of rat neurohypophysis. J Neurosci 22:6891–6899.

Li XF, Kraev AS, Lytton J (2002) Molecular cloning of a fourth member of the potassium-dependent sodium-calcium exchanger gene family, NCKX4. J Biol Chem 277:48410–48417.

Li Z, Hatton GI (1997) Ca^{2+} release from internal stores: role in generating depolarizing after-potentials in rat supraoptic neurones. J Physiol (Lond) 498:339–350.

Li Z, Matsuoka S, Hryshko LV, Nicoll DA, Bersohn MM, Burke EP, Lifton RP, Philipson KD (1994) Cloning of the NCX2 isoform of the plasma membrane Na^+-Ca^{2+} exchanger. J Biol Chem 269:17434–17439.

Markram H, Helm PJ, Sakmann B (1995) Dendritic calcium transients evoked by single back-propagating action potentials in rat neocortical pyramidal neurons. J Physiol (Lond) 485:1–20.

Mironov SL, Usachev YM, Lux HD (1993) Spatial and temporal control of intracellular free Ca^{2+} in chick sensory neurons. Pflügers Arch 424:183–191.

Neher E, Augustine GJ (1992) Calcium gradients and buffers in bovine chromaffin cells. J Physiol (Lond) 450:273–301.

Nicoll DA, Longoni S, Philipson KD (1990) Molecular cloning and functional expression of the cardiac sarcolemmal Na^+-Ca^{2+} exchanger. Science 250:562–565.

Nicoll DA, Quednau BD, Qui Z, Xia YR, Lusis AJ, Philipson KD (1996) Cloning of a third mammalian Na^+-Ca^{2+} exchanger, NCX3. J Biol Chem 271:24914–24921.

Park YB, Herrington J, Babcock DF, Hille B (1996) Ca^{2+} clearance mechanisms in isolated rat adrenal chromaffin cells. J Physiol (Lond) 492:329–346.

Prinsen CF, Szerencsei RT, Schnetkamp PP (2000) Molecular cloning and functional expression of the potassium-dependent sodium-calcium exchanger from human and chicken retinal cone photoreceptors. J Neurosci 20:1424–1434.

Reuter H, Porzig H (1995) Localization and functional significance of the Na^+/Ca^{2+} exchanger in presynaptic boutons of hippocampal cells in culture. Neuron 15:1077–1084.

Sagara Y, Fernandez-Belda F, de Meis L, Inesi G (1992) Characterization of the inhibition of intracellular Ca^{2+} transport ATPases by thapsigargin. J Biol Chem 267:12606–12613.

Sanchez-Armass S, Blaustein MP (1987) Role of sodium-calcium exchange in regulation of intracellular calcium in nerve terminals. Am J Physiol 252:C595–C603.

Stuenkel EL (1994) Regulation of intracellular calcium and calcium buffering properties if rat isolated neurohypophysial nerve endings. J Physiol (Lond) 481:251–271.

Thayer SA, Usachev YM, Pottorf WJ (2002) Modulating Ca^{2+} clearance from neurons. Front Biosci 7:D1255–D1279.

Tsoi M, Rhee KH, Bungard D, Li XF, Lee SL, Auer RN, Lytton J (1998) Molecular cloning of a novel potassium-dependent sodium-calcium exchanger from rat brain. J Biol Chem 273:4155–4162.

Usachev YM, DeMarco SJ, Campbell C, Strehler EE, Thayer SA (2002) Bradykinin and ATP accelerate Ca^{2+} efflux from rat sensory neurons via protein kinase C and the plasma membrane Ca^{2+} pump isoform 4. Neuron 33:113–122.

Werth JL, Thayer SA (1994) Mitochondria buffer physiological calcium loads in cultured rat dorsal root ganglion neurons. J Neurosci 14:348–356.

Zenisek D, Matthews G (2000) The role of mitochondria in presynaptic calcium handling at a ribbon synapse. Neuron 25:229–237.

Zhou Z, Neher E (1993) Mobile and immobile calcium buffers in bovine adrenal chromaffin cells. J Physiol (Lond) 469:245–273.